CONF-8908125--1

THERMAL-SHOCK EXPERIMENTS WITH FLAWED CLAD CYLINDERS*

R. D. Cheverton, J. W. Bryson, D. J. Alexander
Oak Ridge, National Laboratory
Oak Ridge, Tennessee

T. Slot, Consultant

CONF-8908125--1

DE89 016069

---

*Research sponsored by Knolls Atomic Power Laboratory under Martin Marietta Energy Systems, Inc., Contract DE-AC05-84OR21400 with the U.S. Department of Energy.

THERMAL-SHOCK EXPERIMENTS WITH FLAWED CLAD CYLINDERS

R. D. Cheverton, J. W. Bryson and D. J. Alexander
Oak Ridge National Laboratory
Oak Ridge, Tennessee

T. Slot, Consultant

1. INTRODUCTION

The life expectancy of LWR pressure vessels is influenced by a reduction in fracture toughness that is the result of radiation damage. As the fracture toughness decreases, the probability of propagation of preexisting flaws (sharp, crack-like defects) in the wall of the vessel increases. The probability of propagation is also influenced by the type of loading condition and the type of flaws that might exist. A loading condition of particular concern is referred to as pressurized thermal shock (PTS), and a flaw of particular concern for PTS loading conditions is a shallow surface flaw [1].

A sudden cooling (thermal shock) of the inner surface of the vessel results in relatively high tensile stresses and relatively low fracture toughness at the inner surface. In addition, the attenuation of the fast-neutron fluence also results in relatively low fracture toughness at the inner surface. Under some circumstances, this combination of high stress and low toughness at the inner surface makes it possible for very shallow surface flaws to propagate (also referred to herein as crack initiation). In general, shallow (small) flaws are more likely to exist than deep (large) flaws, and thus the concern over shallow surface flaws.

The PTS issue has been under investigation for quite some time, but thus far possible beneficial effects, other than thermal resistance, of the cladding on the inner surface of the vessel have not been included in the analysis of flaw behavior [2,3]. If the cladding has and retains sufficient toughness, the probability of propagation and extent of propagation for subclad flaws and the extent of propagation for surface flaws will be less than that for a surface flaw in the absence of cladding. However, the extent of the benefit of the cladding for subclad flaws depends on (1) the amount of stretching of the cladding above the crack and (2) the critical load for failure (breaching) of the cladding relative to that for the base material. The greater the stretching, the less the benefit; and if the critical load for the cladding is less than for the base material, there is no benefit other than thermal.

Although much emphasis has been placed on surface flaws in the PTS evaluations, there are circumstances that can result in a relatively low probability of the existence of surface flaws compared to subclad flaws. Thus, it is also important to understand the effects of cladding on the behavior of subclad flaws. It may be that a better understanding of the behavior of both surface and subclad flaws in the presence of cladding will result in a longer permissible service life for LWR vessels.

Experimental evaluations of the behavior of surface flaws in the presence of cladding, using mechanically loaded clad plates [4] and beams [5], and irradiation of cladding [6] have been underway since 1981, and more recently (1984) the cladding-effects study discussed herein was begun. This latter study included thermal-shock experiments with a clad cylinder containing both surface and subclad flaws, the development of associated analytical models, and materials characterization studies. A primary purpose of the study was to evaluate the adequacy of the analytical models for predicting the initiation behavior of both subclad and through-clad (surface) flaws under thermal-shock loading conditions. This paper briefly describes the analytical models, discusses five thermal-shock experiments, and compares the analytical and experimental results with regard to the beneficial effects of cladding. The study is ongoing, and thus this account must be considered as preliminary.

2. ANALYTICAL MODELS

The ORMGEN/ADINA/ORVIRT fracture analysis system, which performs static analyses of brittle and ductile fracture in two-dimensional (2-D) and three-dimensional (3-D) geometries, was used for predicting flaw behavior. ORMGEN [7] automatically generates a complete 3-D finite-element model of the cracked structure and creates data files that have formats compatible with the ADINA [8] structural analysis program. ORVIRT [9] acts as a post-processor of conventional ADINA stress analyses. The strategy employed in ORMGEN is to surround the crack front with a core of special wedge-shaped crack-tip elements (Fig. 1) and to model the remainder of the structure with conventional 20-node isoparametric brick elements. The special crack-tip elements model the appropriate singularity in the stress field. The nodes that initially share the same locations at the tip (Fig. 1a) will separate with increasing load to allow for blunting of the crack (Fig. 1b). This feature permits stretching of the cladding above a subclad flaw, and this stretching enhances the stress intensity factor (K_I) along the portion of the crack front in the base material.

The special crack-tip elements indicated in Fig. 1 are applied to the crack front in the base material for 2-D and 3-D surface and subclad flaws and at the clad/base interface for 2-D subclad flaws. Because of mesh-design complexities, crack-tip elements have not been applied to the portion of the crack front at the clad/base interface for 3-D subclad flaws. A correction to the base-material crack-front K_I values, associated with stretching of the cladding, was based on results of two 2-D calculations, one with and one without the crack-tip blunting feature.

A deformation-plasticity-material model was added to the ORNL version of ADINA that utilizes a multilinear, temperature-independent, stress-strain curve. It was also necessary to modify this ADINA

material model, as well as ORVIRT, to handle a second material (cladding). Because stresses in the cladding tend to exceed the yield stress during the thermal-shock experiments, all of the fracture analyses were performed using the elastoplastic model.

The ORVIRT fracture-mechanics program utilizes a virtual-crack-extension technique developed by deLorenzi [10] for isothermal applications and modified by Bass and Bryson [11] to account for thermal strains in cracked bodies.

3. EFFECTS OF CLADDING AND THE CALCULATED BENEFIT FOR A SUBCLAD FLAW

By comparison with an unclad vessel, the presence of cladding (1) reduces the severity of the PTS thermal shock (relatively low thermal conductivity) and thus tends to reduce the potential for propagation of flaws; and (2) introduces high thermal stresses near the surface (relatively high coefficient of thermal expansion) and thus tends to increase the potential for propagation of surface flaws. For a subclad flaw, in effect, the cladding provides a crack-mouth closing force (Fig. 2) that reduces K_I relative to that for a surface flaw. The crack-mouth closing force is essentially equal to the stress in the cladding times the thickness of the cladding [12], and for severe thermal-shock loading conditions this stress is the "yield" stress.

The benefit of the cladding for a subclad flaw can be defined in terms of the reduction in K_I relative to some other specified condition for analysis. One of these other conditions could be a surface flaw in a clad vessel. Calculations for the thermal-shock experiments to be discussed later indicate that for the times of maximum K_I, the K_I value for the subclad flaw is ~34% less. If the yield stress of the cladding were different from that assumed (65 ksi), the benefit of the cladding would be different by about the same percentage. For instance, if the yield stress were 20% less (52 ksi), the cladding benefit would be ~28%.

4. EXPERIMENTS

4.1 Concept and Design

The thermal-shock experiments were conducted with a large (39-in OD × 48-in length), thick-walled (6 in), cylinder of typical LWR vessel material (A508, class-2-chemistry steel). The inner surface was clad with both 304L stainless steel (90° segment) and Inconel 600 (270° segment) (Fig. 3), and both cladding materials were applied with the strip weld (1-in strip), submerged-arc process (strips oriented in a longitudinal direction). Two layers of cladding were applied, and final machining of the clad inner surface reduced the thickness of the cladding to ~0.18 in., relative to the initial surface, and 0.22 in. for the total fusion zone.

The cylinder was in the as-quenched condition when the cladding was applied. Following cladding and after final machining of the inner surface, the cylinder was tempered at 1150°F for 7 h to achieve rather low toughness (RT_{NDT} = 150°F).

Multiple flaws, both subclad and through-clad (surface), were used to (1) improve statistics, (2) include more than one type and size of flaw, and (3) improve cost effectiveness. Interaction effects were determined to be acceptable.

Thermal-shock loading was used because it was the specific loading condition of interest; it can result in propagation of shallow flaws; and the radial positive gradient in temperature permits crack arrest at reasonable depths, allowing more than one experiment with the same cylinder.

The two basic fracture parameters in the experiments were K_I and the static crack initiation fracture toughness (K_{Ic}) of the base material. A comparison of the "calculated" value of K_I/K_{Ic} with unity, the actual value corresponding to crack initiation, provides an indication of the validity of the analytical capability. Values of K_I and K_{Ic} for a specific crack initiation event in the experiment were calculated using the measured temperatures and K_{Ic} data. These latter data were deduced from similar previous thermal-shock experiments [1] and from materials characterization studies associated with the present program. There is considerable uncertainty in the K_{Ic} data (±45%). Mean values equal to 1.8 times the ASME lower-bound curve [13] were used for pre and posttest evaluations (Fig. 4). This mean curve agrees well with the data deduced from the previous thermal-shock experiments.

4.2 Experiment Techniques

4.2.1 Flawing: All flaws were created using the electron-beam (EB)-weld, hydrogen-charge technique [14]. Subclad flaws were generated as surface flaws before application of cladding and then clad over with a cladding strip centered over the flaw (flaws 1-6, Fig. 3). Two through-clad flaws were generated by penetrating the cladding with the EB weld (flaws 7 and 8), and four others were generated by slitting the cladding over a subclad flaw (flaws 2, 4, 5, and 6), following previous experiments with the subclad flaws.

4.2.2 Thermal shock: The thermal-shock was achieved, as in previous experiments [15], by first heating the test cylinder to 200°F and then effectively dunking the test-cylinder assembly in a tank of liquid nitrogen (-320°F). The ends and outer surface of the test cylinder were thermally insulated to confine the thermal shock to the inner surface (Fig. 5), and the inner surface was coated with a thin layer of material that supresses film boiling and promotes nucleate boiling. The thermal conductivities of the two cladding materials are essentially the same; thus, the quench rate was uniform around the cylinder.

4.2.3 Instrumentation: Temperature distributions in the wall were measured at fifteen locations with through-wall thimbles containing twelve thermocouples each [15]. Weldable strain gages were used to measure

surface displacement above subclad flaws and crack-mouth-opening displacement for surface flaws (step changes in output from these gages indicated the time of crack propagation) [15].

4.2.4 Posttest examination: Ultrasonic techniques were used to estimate flaw shape and size; dye-penetrant inspection was performed to check for breaching of the cladding; and visual inspection was performed for detection of stretch zones in the cladding above the flaws. Following the final experiment (TSE-11), the cylinder was cut into pieces for a more direct examination of the flaws (profiles and fracture surfaces).

4.3 Specific Experiments

Four thermal-shock experiments (TSE-8, TSE-9, TSE-10, and TSE-11) were conducted. The corresponding flaws are identified and defined in Figs. 3 and 6 and Table 1.

Table 1. Flaws for each experiment[a]

Exp	Flaw number							
	1	2	3	4	5	6	7	8
TSE-8	*b*	*b*	*b*	*b*	*b*	*b*	–	–
TSE-9	*b*	*b*	*c*	*b*	*b*	*b*	*d*	*d*
TSE-10	*b*	*b*	*c*	*b*	*b*	*b*	*e*	*d*
TSE-11	*b*	*f*	*c*	*f*	*f*	*f*	*e*	*d*

[a]All flaws located at mid length of test cylinder and oriented axially.

[b]Subclad, 6/1 semielliptical, depth from clad/base interface = 0.75 in.

[c]Subclad, extended radially and axially during TSE-8 (~2.8 × 40 in.)

[d]Surface, semicircular, radius = 0.75 in., max depth = 0.95 in.

[e]Surface, extended axially slightly during TSE-9.

[f]Surface, converted following TSE-10.

4.4 Results

4.4.1 Thermal transients: The thermal transients achieved for the four thermal-shock experiments are indicated in Fig. 7. It is apparent that the TSE-11 transient was substantially more severe than the others (the result of small variations in the surface coating from one experiment to another).

4.4.2 Events: Initiation/arrest events achieved are as follows:

TSE-8: Flaw 3 experienced two initiation/arrest events (t = 142 and 219 s). The length extended to ~40 in. and the maximum depth to ~2.8 in. (measured from surface, Fig. 8); one bifurcation took place near the lower end. There were obvious stretch zones in the cladding (Fig. 9), but there was no breaching of the cladding. Flaws 1, 2, 4, 5, and 6 did not propagate; however, slight stretch zones formed in the cladding above all but flaw 1.

TSE-9: Flaw 7 experienced a single event (t = 92 s). It extended ~0.25 in. on one end, tunneling under the cladding slightly. No other flaws extended.

TSE-10: No flaws propagated.

TSE-11: Ten initiation/arrest events took place during TSE-11 and resulted in the subclad crack-extension pattern and approximate flaw depths shown in Fig. 10. The cracking pattern was initially identified by visual observation of stretch zones in the cladding, but the cladding was not breached. The specific events are indicated in Table 2. It is apparent that at 124 and 230 s one flaw triggered another, presumably as a result of stress waves.

Table 2. Events during TSE-11

Flaw	Time (s)				
	86	124	192	230	390
2	E[a]	E			
3		E	E	E	E
4		E			
5		E			
6		E		E	

[a] E indicates initiation/arrest event

5. POSTTEST EVALUATION OF EXPERIMENTS

5.1 Comparison of Results from TSE-8, TSE-9, TSE-10, and TSE-11

A summary of the posttest calculated values of K_I/K_{Ic} corresponding to (1) initiation events and (2) the time at which the maximum value, but not initiation, occurred are presented in Table 3. Corresponding flaw sizes were determined by ultrasonic inspection and also by direct observation of fracture surfaces following TSE-11 (for example, Fig. 11). As mentioned in Sects. 2 and 4, the K_I values were calculated using an elastoplastic model, temperature-independent properties, and the measured temperatures; and K_{Ic} values were obtained from Fig. 4 (mean curve), using the measured temperatures.

The K_I/K_{Ic} values in Table 3 are maximum values along the crack front and, for the surface flaws, correspond to a location in the base-material heat-affected zone (HAZ) at the clad/base interface. There are indications from the materials characterization program and the earlier cladding-effects studies [5] that the HAZ may be somewhat tougher than the adjacent base material. Furthermore, the loading history for the semielliptical surface flaws might have elevated their effective fracture toughness some. If these trends actually exist (they have not been verified), they would result in smaller calculated values of K_I/K_{Ic} for one or both types of surface flaws.

Table 3. K_I/K_{Ic} calculated values corresponding to initiation events or time of maximum value

Flaw[a]	Flaw		Type Cladding[b]	Flaw/TSE	Initiation?	K_I/K_{Ic}[c]
	Shape	Depth				
SC	6/1	(0.75)	I	3/8	Yes	0.8
SC	16/1	(2.3)	I	3/11	Yes	1.0
SC	16/1	(2.3)	I	3/9	No	?
SC	6/1	(0.75)	SS	1/8	No	1.0
SC	6/1	(0.75)	I	2,4,5,6/8	No	1.0
S	2/1	(0.75)	SS	7/9	Yes	1.3
S	6/1	(0.75)	I	2,4,5,6/11	Yes	1.5
S	2/1	(0.75)	SS	7/10	No	1.3

[a] Subclad (SC) and surface(S)

[b] Inconel (I) and stainless steel (SS)

[c] Maximum value on portion of crack front in base material

If the above trends do not exist or are neglible, the deviations from unity may still be explained by uncertainties and scatter in K_{Ic} [all of the "K_{Ic}" values deduced from TSE-8, 9 and 11 fall within the scatter band of data from the previous thermal-shock experiments (Fig. 4)]. However, other possibilities, indicated by the apparent trend in Table 3, are that (1) the assumed values of K_{Ic} are too low for all flaws and (2) the calculational model underestimates stretching of the cladding (overestimates the crack-mouth closing force provided by the cladding) above the subclad flaws and thus underestimates the K_I values for the portion of the crack front in the base material.

The assumed "strength" of the cladding is an important parameter in calculating the effect of the cladding.* For instance, reducing the effective strength increases K_I for the subclad flaws and decreases K_I (by a lesser amount) for the surface flaws. Thus, decreasing the effective strength of the cladding will tend to bring the calculated values of K_I/K_{Ic} in Table 3, corresponding to events, closer together.

5.2 Comparison of Results from TSE-7 and TSE-9

TSE-7 was a similar experiment conducted in an earlier program [1]. The test cylinder was fabricated from the same heat of material but was tempered at a higher temperature to achieve greater toughness (RT_{NDT} = 30°F). The flaw was a 0.75-in.-radius semicircular EB-weld-induced surface crack similar to that for TSE-9, but there was no cladding. The applied thermal shock was the same (200°F initial temperature, quench in liquid nitrogen), and in both cases crack initiation took place. There were three initiation arrest events during TSE-7, and as a result of the first (t = 92 s), essentially the entire surface cracking pattern shown in Fig. 12 developed. The maximum crack depth corresponding to the first event was 1.3 in., and the final depth was 2.3. By comparison, there was a single event during TSE-9 (t = 92 s), and the extension was only 0.25 in. This is a convincing though qualitative demonstration of the benefit of cladding for a surface flaw that initially extends into the base material. To quantify the benefit, it would be necessary to conduct a severe enough TSE-9-type experiment to achieve extensive propagation; this was not accomplished.

6. DISCUSSION AND CONCLUSIONS

Subclad flaws tend to have a smaller potential for propagation into the base material than through-clad (surface) flaws, but the extent of the benefit depends on two factors: (1) the fracture resistance of the cladding and (2) the amount of stretching of the cladding over the flaw. If the cladding is breached at a "load" less than the critical

*Miniature tensile-specimen stress-strain curves for the actual cladding material were used in the analysis.

load for propagation of an otherwise similar through-clad flaw, a structural benefit of the cladding does not exist. If the cladding is not breached, the benefit decreases with increasing stretching (decreasing strength and thus decreasing crack-mouth closing force) of the cladding for a given applied load. For this series of thermal-shock experiments, the cladding was not breached, but calculated values of K_I/K_{Ic} corresponding to initiation events indicate that stretching of the cladding may have been somewhat greater than calculated.

Calculations performed as a part of this study (Sect. 3) indicate that the benefit of the cladding for a subclad flaw relative to a through-clad flaw is a reduction in K_I of ~34%, and that if the yield strength of the cladding were as much as 20% less than measured and used in the calculation, the benefit would still be 28%, which is considered to be substantial.

Although the discrepancies between calculations and experimental results could be attributed to uncertainty and scatter in the fracture toughness of the base material and its HAZ at the clad/base interface, some of the discrepancies could also be attributed to the anaytical model.

A direct comparison of results from thermal-shock experiments with and without cladding present (TSE-9 and TSE-7) indicates an advantage of cladding for surface flaws: the presence of cladding requires a more severe transient for extensive propagation.

REFERENCES

1. Cheverton, R. D., Iskander, S. K., and Ball, D. G., "Review of Pressurized-Water-Reactor-Related Thermal Shock Studies," *Fracture Mechanics: Nineteenth Symposium, ASTM STP 969*, T. A. Cruse, Ed., American Society for Testing Materials, Philadelphia, 1988, pp. 752-766.

2. Cheverton, R. D. and Ball, D. G., "A Reassessment of PWR Pressure Vessel Integrity During Overcooling Accidents, Considering 3-D Flaws," *Journal of Pressure Vessel Technology*, Vol. 106/375, November 1984.

3. Selby, D. L., et al., "Pressurized Thermal Shock Evaluation of the H. B. Robinson Unit 2 Nuclear Power Plant," NUREG/CR-4183 (ORNL/TM-9567), Vols. 1 and 2, Oak Ridge National Laboratory, Oak Ridge, TN, September 1985.

4. Corwin, W. R., Reactor Vessel Cladding Separate Effects Studies, *Nuclear Engineering and Design* 98(1987)171-193.

5. McCabe, D. E., Fracture Evaluation of Surface Cracks Embedded in Reactor Vessel Cladding, NUREG/CR-4841 (MEA-2200), Materials Engineering Associates, Inc., May 1987.

6. Corwin, W. R., et al., Fracture Behavior of a Neutron-Irradiated Stainless Steel Submerged are Weld Cladding Overlay, *Nuclear Engineering and Design 89(1985)199-221.*

7. Bass, B. R. and Bryson, J. W., *Applications of Energy Release Rate Techniques to Part-through Cracks in Plates and Cylinders, Vol. 1. ORMGEN-3D: A Finite Element Mesh Generator for 3-Dimensional Crack Geometries*, NUREG/CR-2997, Vol. 1 (ORNL/TM-8526/V1), Oak Ridge National Laboratory, Oak Ridge, TN (December 1982).

8. Bathe, K. J., "ADINA - A Finite Element Program for Automatic Dynamic Incremental Nonlinear Analysis", Report AE 84-1, ADINA Engineering, Inc., Watertown, MA (December 1984).

9. Bass, B. R. and Bryson, J. W., *Applications of Energy Release Rate Techniques to Part-through Cracks in Plates and Cylinders, Vol. 2. ORVIRT: A Finite Element Program for Energy Release Rate Calculations for 2-D and 3-D Crack Models*, NUREG/CR-2997, Vol. 2 (ORNL/TM-8527/V2), Oak Ridge National Laboratory, Oak Ridge, TN (February 1983).

10. deLorenzi, H. G., "On the Energy Release Rate and the J-Integral for 3-D Crack Configuration", *International Journal of Fracture*, Vol. 19, 1982, pp. 183-193.

11. Bass, B. R. and Bryson, J. W., "Energy Release Rate Techniques for Combined Thermo-Mechanical Loading", *International Journal of Fracture*, Vol. 22, p. R3, 1983.

12. R. D. Cheverton, et al., *Heavy Section Steel Technology Program Quarterly Progress Report for July-September 1981*, NUREG/CR-2141, Vol. 3 (ORNL/TM-8145), February 1982, pp. 91-93.

13. *ASME Code*, Section XI, Division 1, Subsection NB-2331, American Society of Mechanical Engineers, New York, NY.

14. Holz, P. P., "Preparation of Long Axial Flaw for TSE-5A," *Heavy-Section Steel Technology Program Quarterly Progress Report July-September 1980*, NUREG/CR-1806 (ORNL/NUREG/TM-419), Oak Ridge National Laboratory, Oak Ridge, TN, December 1980, pp. 35-37.

15. Cheverton, R. D., et al., "Pressure Vessel Fracture Studies Pertaining to the PWR Thermal-Shock Issue: Experiments TSE-5, TSE-5A, and TSE-6," NUREG/CR-4249 (ORNL-6163), Oak Ridge National Laboratory, Oak Ridge, TN, June 1985.

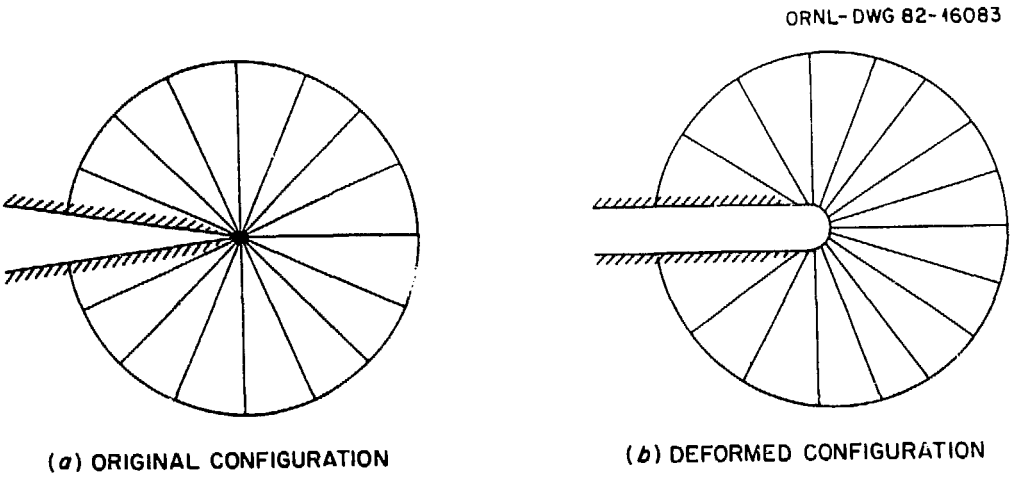

Fig. 1. Collapsed prism elements appropriate for nonlinear analysis.

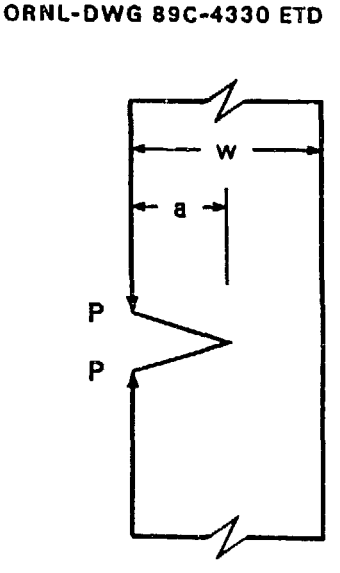

Fig. 2. Crack-mouth closing force associated with tensile stress in cladding over subclad flaw.

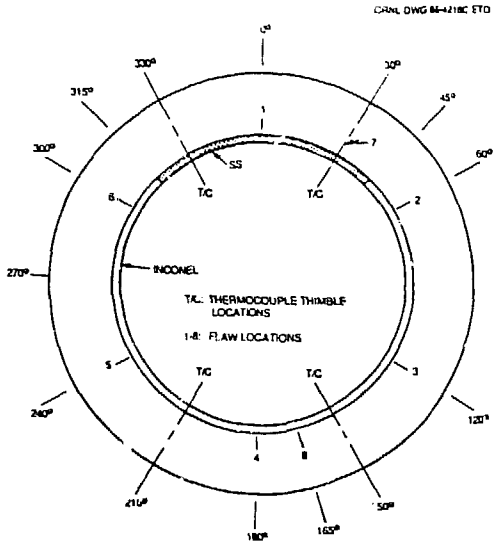

Fig. 3. Cladding configuration and flaws used in test cylinder.

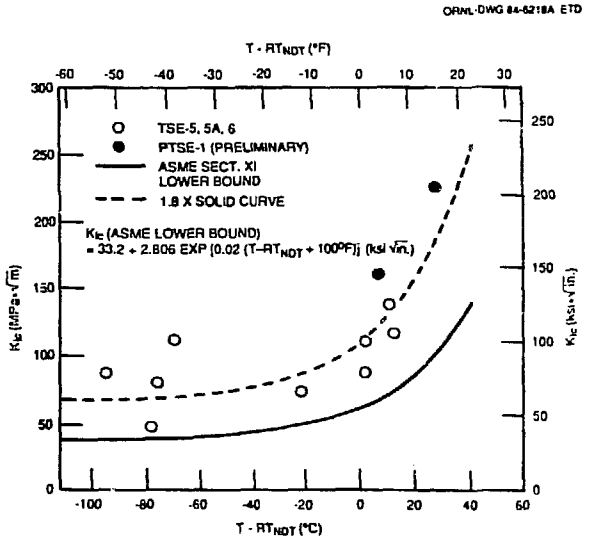

Fig. 4. (K_{Ic} vs T - RT_{NDT}) data deduced from TSE and PTSE experiments.

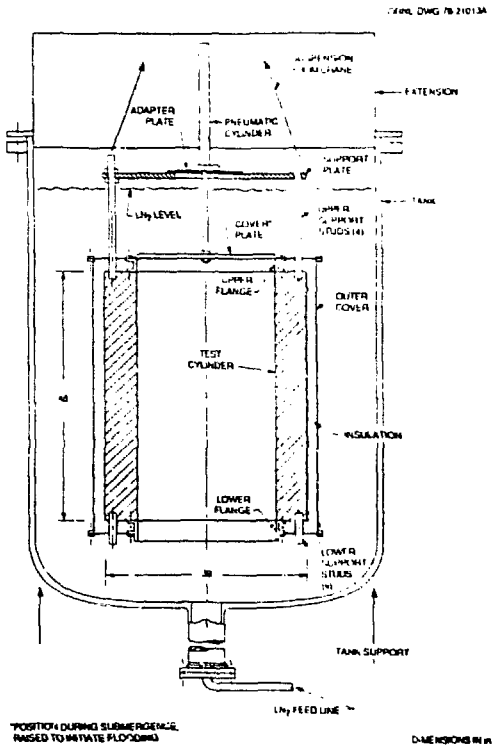

Fig. 5. Liquid-nitrogen thermal-shock test facility.

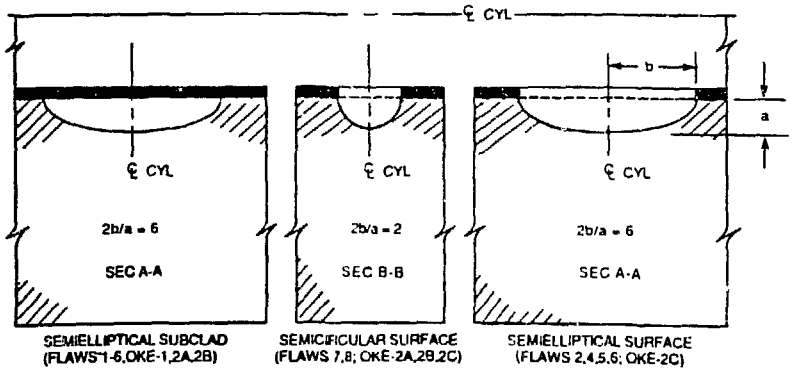

Fig. 6. Types of initial flaws.

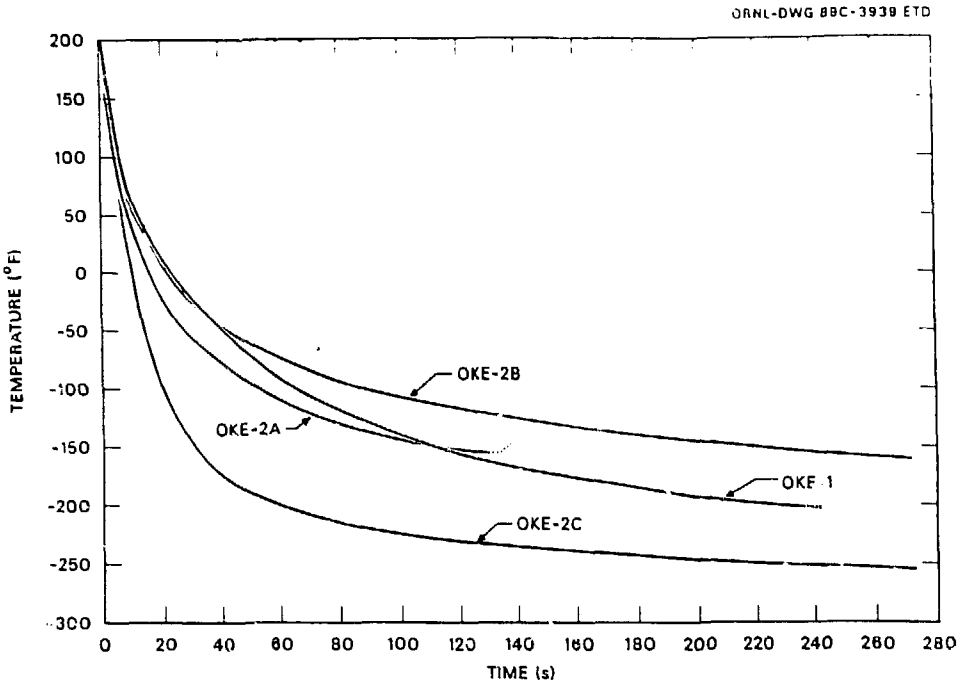

Fig. 7. Comparison of inner-surface temperatures for TSE-8, TSE-9, TSE-10, and TSE-11.

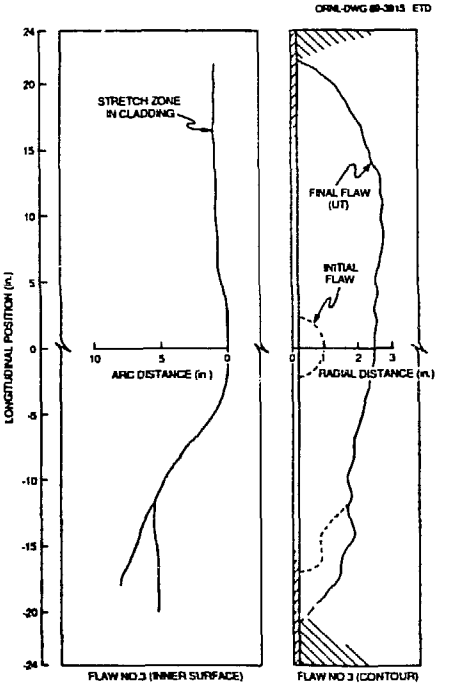

Fig. 8. Stretch-zone and UT indication of flaw 3 TSE-8 extension.

Fig. 9. Stretch zone in cladding above extended flaw 3 (center of stretch zone marked with pen after TSE-8).

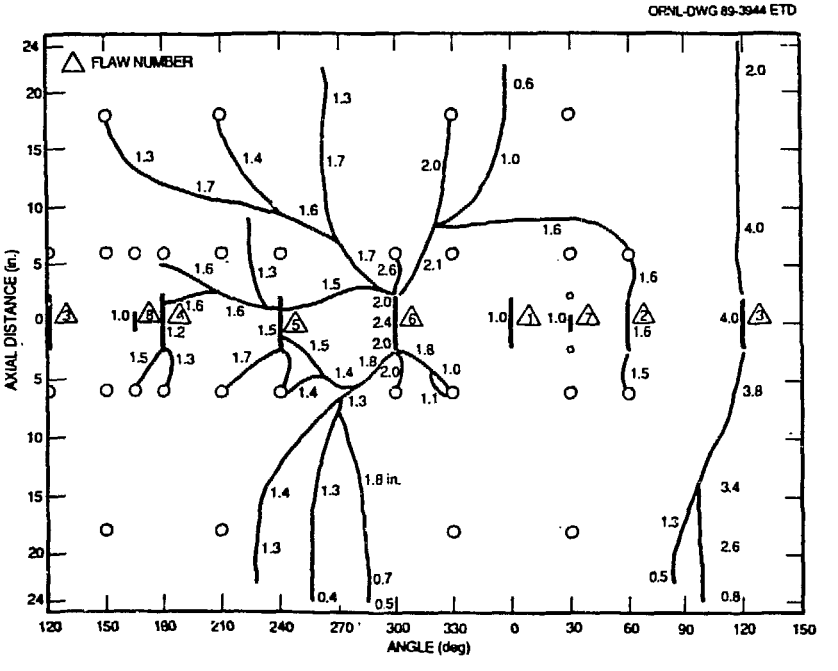

Fig. 10. Tracing of stretch marks in cladding, indicating extent of under-clad crack extension during TSE-8 (flaw 3) and TSE-11, and summary of flaw-depth as obtained by UT inspection (circles represent thermocouple-thimble and crack-arrestor through holes).

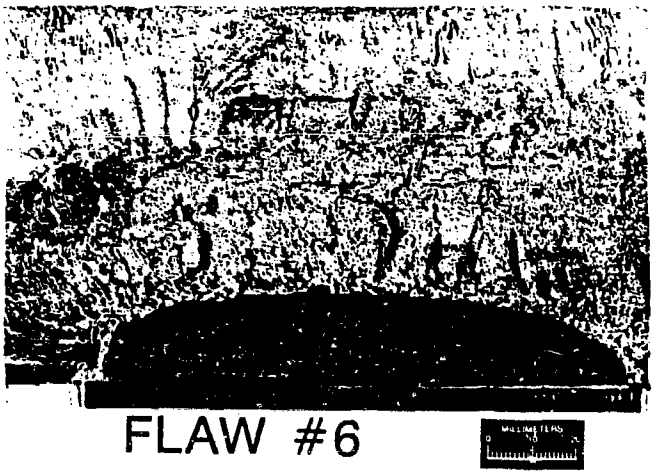

Fig. 11. Fracture surface for flaw 6, indicating initial flaw size (dark area) and machined slit in cladding that converted flaw from subclad to surface status following TSE-10.

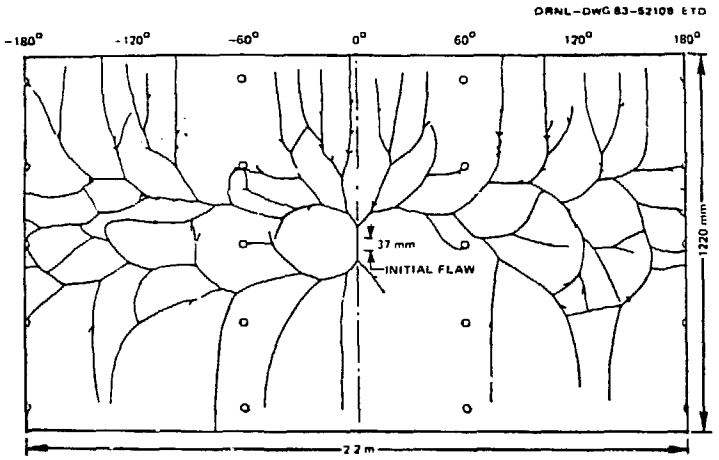

Fig. 12. Developed view of inner surface of TSE-7 test cylinder showing final crack pattern.